

Decomposition of Carbon-Containing Compounds on Solid Catalysts for Single-Walled Nanotube Production

Daniel E. Resasco,* José E. Herrera, and Leandro Balzano

School of Chemical Engineering and Materials Science, University of Oklahoma, Norman, Oklahoma, USA

Different catalyst formulations and reaction conditions have been used to test the validity of a hypothesis that tries to elucidate the mechanism of single-walled nanotube (SWNT) formation by CO disproportionation over a highly selective cobalt-molybdenum catalyst. This model proposed an intrinsic dependence between the selectivity of the catalysts toward SWNT and the stabilization of Co species in a nonmetallic state, which in turn results from an interaction with Mo. The series of tests performed to examine this model include the doping of this highly selective catalyst with sodium, the substitution of molybdenum by tungsten in the original catalyst formulation, the variation on reaction temperature, and the introduction of hydrogen in the gas feedstock. All these modifications were carried out to modify the growth conditions in which the SWNTs are formed. The results are consistent with the hypothesis proposed by the authors.

Keywords: Author, please supply keywords.

[AU:
Please
supply
keywords]

1. INTRODUCTION

The large-scale production of single-walled nanotubes (SWNTs) at low cost is a goal for many research and development groups around the world. Among the various approaches being investigated, the catalytic decomposition of carbon-containing compounds on supported solid catalysts is a synthesis method that could be amenable to the development of continuous processes under relatively mild operating conditions and therefore lower costs than those of the current production methods.¹ However, although the use of supported solid catalysts in the so-called chemical vapor deposition (CVD) method has been widely investigated, the resulting product has exhibited, in most cases, low selectivity to SWNTs and a high density of imperfect multi-walled nanotubes (MWNTs) and nanofibers. Our group has obtained promising results by the disproportionation of CO (decomposition into C and CO₂) over silica-supported Co–Mo catalysts in the temperature range of 700–950 °C.² In previous studies,^{2,3} it was proposed that a synergism between Co and Mo is critical for the performance of this catalyst. If separated, these metals are not effective; they are either inactive (Mo alone) or unselective (Co alone). The catalyst is only effective when both metals are simultaneously present with a low Co:Mo ratio. Through a detailed characterization that involved a variety of characterization techniques such as extended X-ray absorption

fine structure (EXAFS), X-ray absorption near-edge spectroscopy (XANES), ultraviolet/visible (UV/Vis)-diffuse reflectance spectroscopy (DRS), X-ray photoemission spectroscopy, and diffuse reflectance infrared Fourier transform spectroscopy of adsorbed NO, we were able to explain the reasons for the high selectivity of these catalysts.³

A supported metal particle is highly susceptible to aggregation by sintering when it is subjected to the high temperatures needed for the synthesis of SWNTs. A rule of thumb to determine the onset of rapid sintering is the so-called Tamman temperature (one-half the melting point temperature in K).⁴ Accordingly, metals usually used in SWNT synthesis, such as Ni and Co, would rapidly sinter on any support at temperatures above 590 and 610 °C, respectively. These temperatures are much lower than those needed for the synthesis of SWNT. Therefore, one cannot have reduced metal particles on a support before starting the synthesis process because by the time the nanotube growth starts the metal particles will be too large to catalyze the growth of SWNTs. Even when the metal particles may have had nanometric dimensions before the growth started, they quickly sinter at the high temperatures needed for SWNT synthesis.^{5,6} Large metal clusters are known to catalyze the growth of defective MWNTs and nanofibers.⁷ The growth of these forms of carbon follows a well-known mechanism, which has been documented extensively in the past.⁸ That is, the C deposited on the surface of the metal particles begin to dissolve into the particle, which then precipitates graphite in the form of cylindrical filaments. In contrast, when the

*Author to whom correspondence should be addressed.

metal clusters are so small that they are only composed by a few atoms, a different mechanism must be considered.⁹

When precautions to avoid metal sintering during the CVD process are not taken, particles of a broad distribution of sizes are produced and the selectivity toward SWNT is drastically reduced. Therefore, although SWNTs are produced in many CVD processes, only a few are able to produce SWNTs with high selectivity (i.e., low production of undesired forms of carbon). To avoid particle sintering, Laurent et al.¹⁰ and our research group^{2, 3, 11} have independently designed catalysts, which have the common characteristic of being produced only under reaction conditions. Solid oxide solutions such as $Mg_{1-x}Co_xO$ or silica-supported Co–molybdates have been found to be effective catalysts when they are reduced *in situ* by the same carbon-containing reactant that produces the SWNT. Only under specific conditions and using the proper catalyst formulation can SWNT with high selectivity be produced.

In the case of the Co–molybdate catalysts, the selectivity toward SWNT production strongly depends on the stabilization of Co^{2+} species by Mo oxide species. We found that the extent of the Co–Mo interaction is a function of the Co:Mo ratio in the catalyst and has different forms during the different stages of the catalyst life.^{3, 11} In the calcined state, Mo is in the form of a well-dispersed $Mo(6+)$ oxide, whereas the state of Co strongly depends on the Co:Mo ratio. At low Co:Mo ratios, it interacts with Mo in a superficial Co–molybdate-like structure. At high Co:Mo ratios, it forms a noninteracting Co_3O_4 phase. During the subsequent reduction treatment in hydrogen, the noninteracting Co phase is reduced to metallic Co, whereas the Co–molybdate-like species remain as well-dispersed Co^{2+} ions. This Co–Mo interaction inhibits the Co sintering that typically occurs at the high temperatures required for the formation of carbon nanotubes. When large Co particles are present, less desirable forms of carbon (mostly graphitic nanofibers) are produced. In contrast, when the Co clusters are so small that they are only composed by a few atoms, only SWNTs are produced.

When metal atoms begin to agglomerate in the presence of gaseous CO, there is a nucleation period over which there is no growth of nanotubes. This nucleation involves the disruption of Co atoms from its interaction with Mo oxide when the latter becomes carbidic. This disruption is followed by surface migration, leading to agglomeration into mobile clusters that continue to grow under the bombardment of CO molecules.

Some of these molecules decompose and begin to rearrange (nucleate) until a given configuration and carbon surface concentration are reached, which favor the formation of the nanotube. In previous work we proposed calling this configuration the *embryo*. When this embryo is formed, the subsequent incorporation of carbon and SWNT formation would proceed at a fast rate, perhaps only controlled by mass transfer. As a result, one may conclude that the

growth of each nanotube is limited by nucleation, and after nucleation is completed, it is controlled by mass transfer. For this reason, we observed that the deposition of carbon on a solid catalyst continues for hours, although the growth of a single nanotube only takes milliseconds.¹² The diameter of the nanotube is determined by the size of the embryo; therefore, control of nanotube diameter is in principle possible by control of the size of the metal cluster.

In this article we have tested this hypothesis with a series of experiments. In two of these experiments we have varied the catalyst formulation; in the other two, we have varied the growth conditions (i.e., feed and temperature). These experiments are the following.

(a) *Testing a bimetallic system that is chemically similar to Co–Mo.* That is, we have chosen Co–W that is able to form Co–tungstate after treatment in air as well as tungsten carbide after treatment in CO, thus breaking the Co–W interaction under nanotube growth conditions.

(b) *Breaking up the Co–Mo interaction by introducing an element such as Na that will compete with Co for the formation of a Na–molybdate.* Based on the model that we propose, we expect that the addition of Na should have a negative effect on nanotube selectivity.

(c) *Varying the growth temperature.* Here, according to the model, one would expect that, after Co–metal clusters have been formed under reaction conditions, their rate of agglomeration will increase with the growth temperature. Therefore, because the diameter of any given nanotube is determined by the size of the Co–metal cluster that originates it, the higher the growth temperature is, the larger the nanotube diameter is expected to be.

(d) *Incorporating hydrogen in the feed.* It is known that the presence of hydrogen in the gas phase greatly reduces the fugacity of carbonaceous species on the surface. One would expect that this reduction in surface fugacity would delay the nanotube growth by delaying the nucleation process. If that is the case, in the competition between metal cluster agglomeration and nanotube growth, the former would be favored. As a result, depending on the hydrogen concentration, we may observe an increase in nanotube diameter at low H_2 concentrations or even a loss in nanotube selectivity compared with nanofibers when the particle diameter becomes too large to form embryos able to grow SWNTs.

2. EXPERIMENTAL

2.1. Materials and Treatments

The synthesis of SWNTs using a highly selective Co–Mo catalyst has been previously reported.^{3, 13} In brief, the SWNT samples were obtained using a supported bimetallic Co–Mo catalyst with a total metallic loading of 2 wt % and a Co:Mo molar ratio of 1:3. Before the production of SWNTs by CO disproportionation, the Co–Mo catalyst

was heated in H₂ flow to 500 °C and then in He flow to the reaction temperature (700–950 °C) at 10 °C/min. The CO disproportionation reaction used for the production of SWNTs was conducted in the temperature range of 700–950 °C in flow of pure CO at a total pressure between 1 and 5 atm. After nanotube growth the reactor was allowed to cool to room temperature in He flow. The preparation of a selective Co–W/SiO₂ catalyst has also been reported¹³; the activation sequence and the reaction temperature are similar to those described above for the Co–Mo catalyst. To prepare the Na-doped catalyst, a silica support previously doped with 4 wt % of sodium was used. The reaction conditions for the doped catalyst were the same as those mentioned above for the highly selective Co–Mo/SiO₂ catalyst. Finally, the incorporation of hydrogen to the feed was achieved by premixing pure CO with controlled amounts of H₂ by means of mass flow controllers.

2.2. Single-Walled Nanotube Characterization

To characterize the SWNTs, we have used a combination of transmission electron microscopy (TEM), Raman spectroscopy, and temperature programmed oxidation (TPO).

Raman spectroscopy is a particularly powerful technique for characterizing the structure of carbon nanotubes. The tangential mode G-band appearing in the 1400–1700 cm⁻¹ region is related to the Raman-allowed phonon mode E_{2g} and involves out-of-phase intralayer displacement in the graphene structure of the nanotubes. It provides information about the electronic properties of the tubes and is a measure of the presence of ordered carbon. The so-called D band at around 1350 cm⁻¹ is related to defects or to the presence of nanoparticles and amorphous carbon.¹⁴ Although pure SWNTs also have some contribution in this region,¹⁵ the D band provides an indication of the level of disordered carbon. Hence, the size of the D band relative to that of the G band can be used as a qualitative measurement for the formation of undesired forms of carbon. Finally, information about the distribution of tube diameters can be obtained from the analysis of the radial A_{1g} breathing mode (RBM) frequency range, as shown below.¹⁶ Although Raman spectroscopy is very useful for a qualitative analysis, in our case it cannot provide a quantitative account of the different types of SWNTs produced; indeed, it cannot reveal the exact amount of SWNTs present in the samples. On the other hand, TPO can provide a quantitative measure of the carbon yield and selectivity. For instance, we have previously shown that under the TPO conditions and while still immersed in the Co–Mo catalyst, the SWNTs get oxidized in a relatively narrow temperature range, which lies below the temperature in which MWNT, graphite, and carbon fibers are oxidized, but above the temperature at which amorphous and chemically impure carbon species are oxidized.²

3. RESULTS AND DISCUSSION

3.1. Bimetallic Co–W System Analogous to Co–Mo

Because of the strong chemical similarities between Mo and W, comparable catalytic activities can be predicted for the Co–Mo and Co–W catalysts. Based on detailed characterization results we have put together a detailed picture of the structure of this catalyst under reaction conditions and built up an analogy with the Co–Mo system.

The characterization of the Co–W catalyst provides evidence for strong similarities and some interesting differences with the Co–Mo system described above. For instance in Table I the results of the analysis by optical absorption of the energy band gap of tungsten oxide species present in the catalyst are reported. It has been shown that the energy band gap of metal oxides decreases as the domain size increases.¹⁷ Consequently, a comparison can be made between the energies determined on the catalysts under investigation and those on references of known domain size. It is clear that, similar to the case of Mo, in the calcined catalyst,³ W is in an octahedral environment and in the 6+ oxidation state. Furthermore, from the values of the adsorption edge energy, it can be concluded that the tungsten oxide species are forming small well-dispersed clusters with average domain size close to that of the metatungstate ion.¹⁷

The optical absorption spectrum of the Co–W catalysts also presented bands in the 500–600 nm range. These bands are ascribed to d-d transitions [⁴T_{2g} → ⁴A_{2g} and ⁴T_{2g} → ⁴T_{1g} (P)] of high-spin octahedral Co complexes.^{18, 19} The bands corresponding to the bimetallic catalyst appeared at the same position as those corresponding to an analytical sample of CoWO₄. This result indicates that most of the Co is in an octahedral environment forming a cobalt tungstate. Indeed, bands corresponding to Co–O–W stretching modes were detected by Raman spectroscopy. More conclusive evidence is presented in Figure 1. In this case, the X-ray absorption profile of the Co K-edge (E_o = 7709 eV) line is presented for a Co–W (1:3)/SiO₂ catalyst and an analytical sample of CoWO₄. It is clear that in the catalyst the Co is located in an environment similar to that of the CoWO₄, that is, closely interacting with W. However, the slight but clear differences between the spectra of the catalyst and the CoWO₄ reference suggest that the similarity is limited to the local environment around Co and the nature of the ligands, but probably not beyond the first layer of neigh-

Table I. Gap energy values as obtained by UV/Vis-DRS for three W (VI) species with different domain sizes compared with the gap energy value obtained for a Co–W (1:3)/SiO₂ catalyst.

Compound	Gap energy (eV)
WO ₃	2.4
(NH ₄) ₁₀ W ₁₂ O ₄₁	3.0
Na ₂ WO ₄	4.6
Co–W (1:3)/SiO ₂ catalyst	2.9

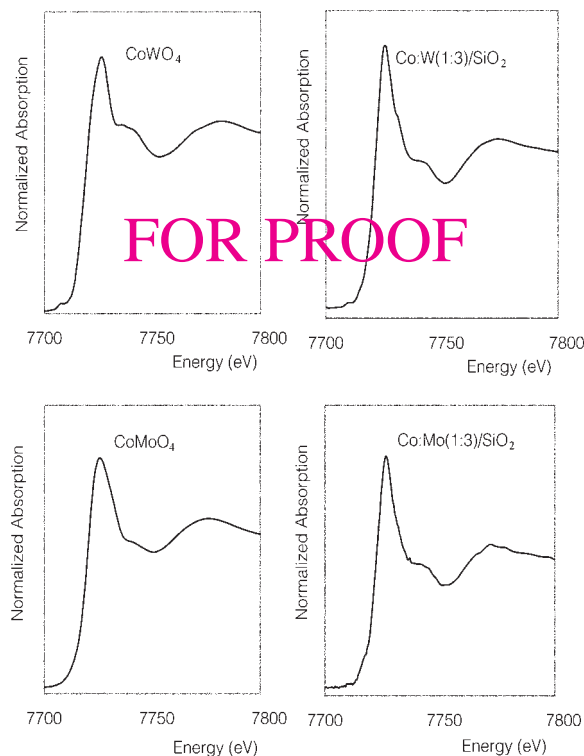


Fig. 1. Co K edge (7709 eV) XANES of a Co–W (1:3)/SiO₂ catalyst, an analytical sample of CoWO₄, a Co–Mo (1:3)/SiO₂ catalyst, and an analytical sample of CoMoO₄ used as a reference.

bors. In fact, the EXAFS data demonstrated that bulk CoWO₄ was not present in the bimetallic catalysts.

When these results are put together in a simple model it is clear that we have achieved on the Co–W catalyst a configuration similar to the one we used to describe the Co–Mo catalytic system. Therefore, we can safely assume that in the Co–W catalysts, dispersed Co species are stabilized over the tungsten oxide in the form of a Co–tungstate-like layer.¹³ This phase will most likely play a determining role in the catalytic activity toward the formation of SWNTs in the same way that the Co–molybdate structure did in the Co–Mo silica catalysts.

Figure 2 shows the product obtained over this Co–W catalyst compared with the product obtained over a selective Co–Mo catalyst at 850 °C by CO disproportionation. The yield of carbon species obtained over the Co–W and the highly selective Co–Mo catalyst is also indicated; it can be observed that although under the right conditions a Co–W catalyst shows a relatively high activity toward SWNT formation, the carbon yield per metal atom and the product quality (D/G band area ratio) for the Co–Mo catalyst are superior. In the case of the Co–Mo system the catalyst was activated at 500 °C in H₂, whereas for the Co–W catalyst the activation step had to be carried out at 900 °C in hydrogen. Notice that the Co–W catalyst requires more severe conditions for activation, mainly due to the high refractoriness of the Co–tungstate species.¹³ We have pre-

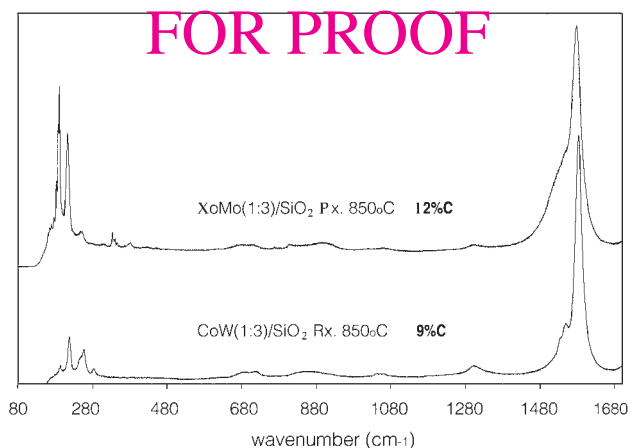


Fig. 2. Raman spectra of the carbon deposits obtained over a Co–W (1:3)/SiO₂ catalyst by disproportionation of CO at 850 °C compared to the Raman spectra obtained for the carbon deposits obtained by CO disproportionation over a highly selective Co–Mo (1:3)/SiO₂ catalyst. The laser excitation line was 633 nm. The yield of carbon deposits as obtained by TPO is also indicated.

viously proposed that a certain degree of reduction associated with the creation of oxygen vacancies around Mo (or W) is necessary because a catalyst that is fully oxidized before the reaction is not efficient.² Indeed when the temperature-programmed reduction profiles of these two different catalysts are compared (Fig. 3), it is clear that the onset of reducibility starts at higher temperatures for the Co–W catalyst than for the Co–Mo catalyst. Regardless of these differences in the required activation temperatures, it is evident that both Co–Mo and Co–W catalytic systems have similar activity toward SWNT formation.

3.2. Breaking the Co–Mo Interaction

Because in our proposed model the interaction of Co and Mo (in the form of cobalt molybdate) is critical for good

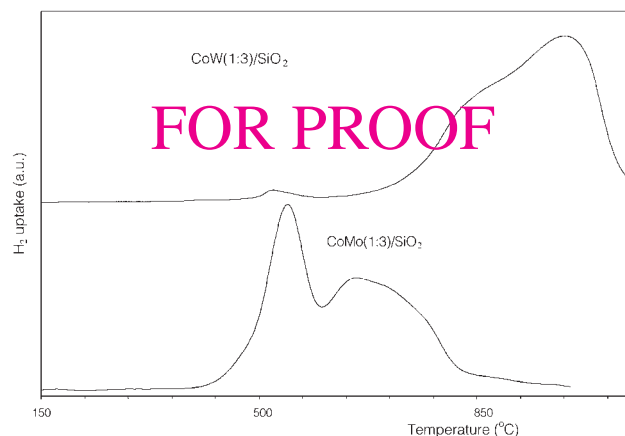


Fig. 3. TPR profiles obtained for a bimetallic cobalt/tungsten catalyst compared to the profile obtained for a Co–Mo (1:3)/SiO₂ catalyst. The TPR was conducted with 5% H₂/Ar at a heating rate of 8 °C/min.

Table II. Gap energy values as obtained by UV/Vis-DRS for three Mo(VI) species with different domain sizes compared with the gap energy values obtained for an undoped and a Na-doped Co–Mo (1:3)/SiO₂ catalyst.

Compound	Gap energy (eV)
MoO ₃	2.6
(NH ₄) ₆ Mo ₇ O ₂₄	3.1
Na ₂ MoO ₄	4.1
Co–Mo (1:3)/SiO ₂ catalyst	2.9
Na-doped Co–Mo (1:3)/SiO ₂ catalyst	3.9

catalyst performance, the introduction of an element that will compete with Co for the formation of the molybdate is expected to be detrimental for the catalytic selectivity. To test this supposition we prepared a catalyst formulation doped with sodium. Before running the reaction, a series of analyses were performed to ensure that the cobalt molybdate structure was broken by the addition of Na. We carried out the first of these tests by optical absorption. Table II reports the results of the energy band gap of molybdenum oxide species present in the Na-doped and undoped catalyst, compared with the gap energy of references of known domain size. The difference in the values obtained for the doped and undoped catalyst is remarkable. It is evident that the undoped catalyst shows values corresponding to Mo located in an octahedral environment whereas the Na-doped catalyst values are close to the gap energy of Mo located in a ligand field of tetrahedral symmetry. Moreover, the optical absorption spectra in the 500–600 nm Co range also showed significant differences. Whereas the undoped catalyst showed bands ascribed to d-d transitions of high-spin octahedral Co complexes, the Na-doped catalyst showed a spectrum of different shape, compatible with Co located in a tetrahedral field. This environment is consistent with the structure of cobalt oxide, in which Co(+2) species are located in the interstices of a spinel structure.

Table III. Observed Raman bands for an undoped Co–Mo (1:3)/SiO₂ catalyst and for a Na-doped Co–Mo (1:3)/SiO₂ catalyst.^a

Sample	Raman bands observed (cm ⁻¹)	Assignment
Undoped Co–Mo (1:3)/SiO ₂ catalyst	348	Mo–O–Co stretching ^{22–25}
	379	
	826	Antisymmetric stretching of Mo–O–Mo in polymeric MoO _x species ^{17, 18} Mo–O–Co stretching ^{22–25}
	880	
	941	
Na-doped Co–Mo (1:3)/SiO ₂ catalyst	198	F _{2g} phonon in Co ₃ O ₄ ¹⁶
	318	
	344	
	478	E _g phonon in Co ₃ O ₄ ¹⁶
	682	F _{2g} phonon in Co ₃ O ₄ ¹⁶
	808	Mo–O–Mo asymmetric stretching in Na ₂ Mo ₄ ¹⁷
	880	Antisymmetric stretching of Mo–O–Mo in polymeric MoO _x species ^{17, 18}
	890	Mo=O stretching in Na ₂ Mo ₄ ¹⁷

^aThe band assignments are based on previously reported values as indicated by the reference numbers. The laser excitation energy was 633 nm.

To confirm these results, Raman spectroscopy was performed on the Na-doped and undoped catalysts. Table III shows the observed bands and their assignment based on previously reported literature. First, it is clear that in the undoped catalyst segregated cobalt species are not present, as evidenced by the lack of the characteristic bands of Co₃O₄ (198, 478, and 682 cm⁻¹).²⁰ The peaks present in the 750–1000 cm⁻¹ region should be ascribed to Mo species. This is the region where the Raman bands for stretching of Mo–O bonds are expected to appear.²¹ A tentative assignment can be made in light of the results obtained by UV/Vis absorption spectroscopy and preceding experiments reported in the literature. For instance, the band at 880 cm⁻¹ is due to the antisymmetric stretching of a bridged Mo–O–Mo structure in polymeric MoO_x species^{21–25}; the Raman bands at 941 and at 350 cm⁻¹ are assigned to Mo–O–Co stretching vibrations in cobalt molybdate species.^{26–29}

A remarkable difference is observed in the band positions of the Raman spectrum of the Na-doped catalyst. New peaks at 198 and 682 cm⁻¹ are present; these two bands correspond to F_{2g} phonon modes of Co₃O₄ whereas the peak at 478 cm⁻¹ is the E_g phonon mode of the same species.²⁰ In agreement with the results obtained by optical absorption, it is clear that Co₃O₄ is the predominant cobalt species present in the Na-doped catalyst. It is also essential to mention that in addition of these three bands, the Raman spectrum of the doped catalyst shows bands at 808 and 890 cm⁻¹, which should be assigned to the stretching of Mo–O–Mo and Mo=O species in Na₂MoO₄, respectively.²¹

These results clearly show that the interaction between Co and Mo in the form of Co–molybdate has been disrupted by the presence of Na. We have proposed that the ability of a Co–Mo catalyst to form SWNTs depends on the formation of this surface Co–molybdate. Therefore, according to our hypothesis, the catalyst doped with sodium should show a low selectivity. Figure 4a shows the Raman spectra

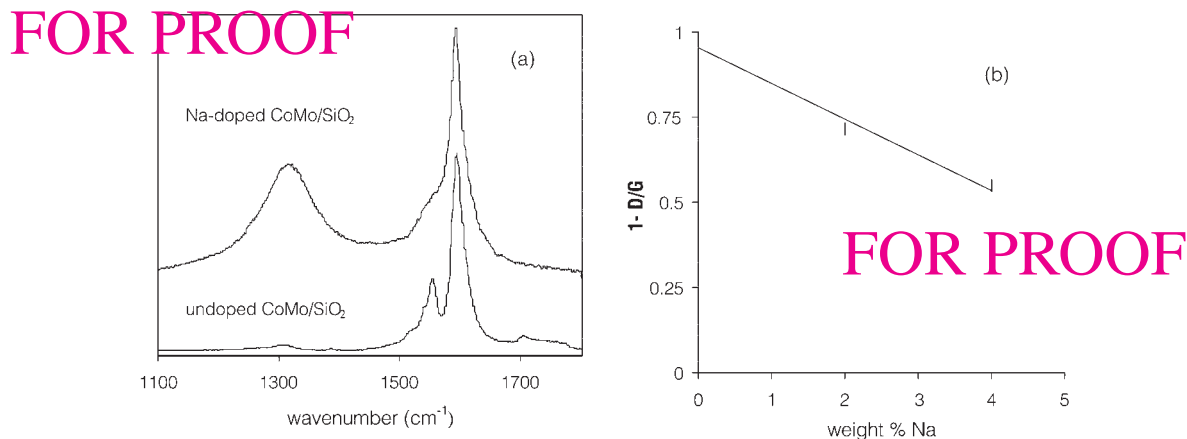


Fig. 4. (a) Raman spectra in the tangential mode region for the carbon deposits obtained over an undoped and a Na-doped Co–Mo (1:3)/SiO₂ catalyst. (b) Contributions of the D band to the Raman spectra of the carbon deposits obtained over three catalysts with different amounts of Na dopant. The contributions of the D band to the Raman spectra are expressed using a quality parameter: $1 - D/G$; where D and G are the integrated areas of the D and G Raman bands, respectively. The laser excitation line was 633 nm.

of the SWNTs obtained using the Na-doped and undoped catalysts. As mentioned above, the tangential Raman mode (G band) appearing in the 1400 – 1700 cm⁻¹ region can be used as a measure of the presence of ordered carbon, whereas the so-called D band at around 1350 cm⁻¹ is related to defects or the presence of nanoparticles and amorphous carbon.¹⁴ A clear difference is observed when the product from an undoped catalyst is compared with that of the Na-doped catalyst. It is clear that the D band contribution becomes much stronger in the spectrum of the product obtained using the Na-doped catalyst than in the spectrum of the undoped sample. This trend is better illustrated in Figure 4b, which shows the gradual decrease of the D band in terms of the expression $(1 - D/G)$ as a function of the Na loading. This term may be considered a “quality parameter” of the SWNT sample, because it qualitatively measures the amount of SWNTs compared with other disordered carbon species. In Figure 4b the quality parameter for a mild Na-doped catalyst is also included; in agreement with our hypothesis the value obtained for this sample falls between the values of the undoped and heavily Na-doped catalyst.

3.3. Varying the Growth Temperature

We conducted the decomposition of CO at temperatures ranging from 750 to 950 °C over a highly selective Co–Mo/SiO₂ catalyst to study the effect of the rate of agglomeration of the Co metal clusters on the SWNT diameter. We had previously shown that although the amount of carbon deposited is larger at 600 °C than at higher temperatures (e.g., 700–800 °C), the selectivity greatly decreased at low temperatures due to the formation of larger fractions of MWNTs and fibers.¹¹ The yields obtained at temperatures between 700 and 850 °C are similar; however, the yield drops when the reaction is run at 950 °C. Here, we

report more subtle changes observed by Raman spectroscopy and TEM. As mentioned above, Raman spectroscopy is particularly useful for this purpose because the nanotube diameter can be calculated from the frequency of the RBM Raman band.¹⁶

Figure 5 shows the Raman spectra (excitation wavelength 514 nm) of SWNT materials obtained at three different temperatures. The product obtained at 750 °C exhibits a dominant peak centered at around 268 cm⁻¹, which would correspond to a nanotube diameter of approximately 0.9 + 0.05.³⁰ However, accurate estimates can only be obtained if intertube coupling is considered, because a significant upshift of the RBM is observed for nanotubes in bundles with respect to isolated nanotubes.³¹ When the temperature was increased to 850 °C a new peak came out at lower wavenumbers (189 cm⁻¹) and when the temperature was increased to 950 °C the main peaks appeared at 236 and

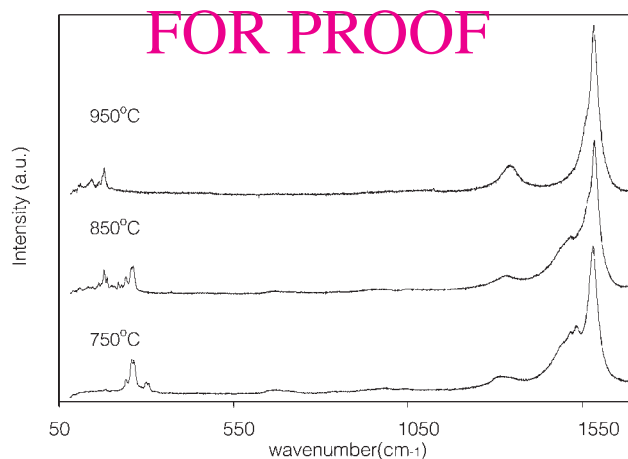


Fig. 5. Raman spectra of the carbon deposits obtained by disproportionation of CO at 750, 850, and 950 °C over a highly selective Co–Mo (1:3)/SiO₂ catalyst. The laser excitation line was 633 nm.

Table IV. Observed radial breathing mode Raman bands for the SWNT obtained by disproportionation of CO at three different temperatures over a Co–Mo (1:3)/SiO₂ catalyst.^a

Laser line	Reaction temperature					
	750 °C		850 °C		950 °C	
	RBM position (cm ⁻¹)	Diameter (nm)	RBM position (cm ⁻¹)	Diameter (nm)	RBM position (cm ⁻¹)	Diameter (nm)
633 nm	284	0.83	257	0.92	188	1.29
	256	0.92	217	1.10	156	1.57
	237	1.00	192	1.26	151	1.63
514 nm	268	0.88	268	0.88	187	1.30
	307	0.76	187	1.30	157	1.56
	251	0.94	251	0.94	130	1.92
488 nm	307	0.76	260	0.91	150	1.64
	261	0.91	244	0.97	120	2.09
	245	0.97	206	1.17		

^aThe laser excitation lines were 633, 514, and 488 nm.

180 cm⁻¹. The positions of these bands indicate that the SWNTs produced at 850 °C have diameters of 0.9 and 1.3 nm, whereas those obtained at 950 °C, have diameters around 1.3 and 1.7 nm. However, because the Raman intensity is strongly affected by resonance phenomena, the radial breathing mode peaks obtained at a fixed laser energy do not reflect the entire diameter distribution of the sample, but rather the subset of nanotubes that are in resonance with the laser photons. Therefore, to get information that is more representative of the diameter distribution of the SWNTs in the sample, it is necessary to probe the SWNT with several excitation energies. Table IV shows the breathing mode range of frequencies in the Raman spectra obtained with three different laser excitation energies on the same SWNT samples. As expected, the peak positions for a given sample are quite different, depending on the laser excitation energy used, but the same trend is observed at all energies. That is, the bands clearly shift to lower wavenumbers as the reaction temperature increased. Because the frequency of the radial breathing mode is inversely proportional to the nanotube diameter,³⁰ this shift indicates an increase in diameter as temperature increases.

To corroborate these results, a detailed analysis by TEM was performed on these series of samples. Figure 6 shows a typical TEM picture obtained on a sample synthesized at 750 °C on a Co–Mo (1:3)–SiO₂ catalyst. It is interesting to note the small metal clusters that appear intermingled with the nanotubes and have about the same diameter as the nanotubes. A small number of larger metal particles are also observed, but they do not seem to be associated with the nanotubes. We need to emphasize also that during the TEM analysis of these sample series we did not find any double- or triple-walled nanotubes. Although some reports indicated that an increase in the metal cluster size results in the formation of these species,^{10, 32} we did not observe them.

We conducted a detailed analysis on several of these TEM micrographs obtained by measuring the diameters of 100–150 nanotubes for each sample. The results of those measurements are summarized in Figure 8. The observed distribution matches the Raman results. The results leave no doubt that as the reaction temperature increased the diameter of the nanotubes increased. This result is in agreement with our growth hypothesis. As proposed above Co atoms start to agglomerate to form mobile clusters, which lead to embryos that result in the growth of SWNT and because the sintering of Co clusters accelerates with temperature, a higher density of larger metal clusters should occur on the catalyst surface as temperature is increased. These larger clusters are then responsible for the formation of larger embryos, and, in turn, nanotubes of larger diameter.

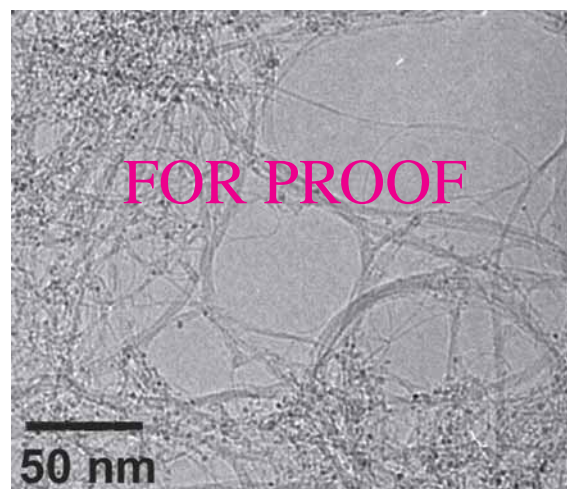


Fig. 6. Typical TEM micrograph of SWNTs produced by CO disproportionation at 850 °C on a Co–Mo catalyst during 2 h. The carbon yield on this sample is approximately 15 wt % C.

FOR PROOF

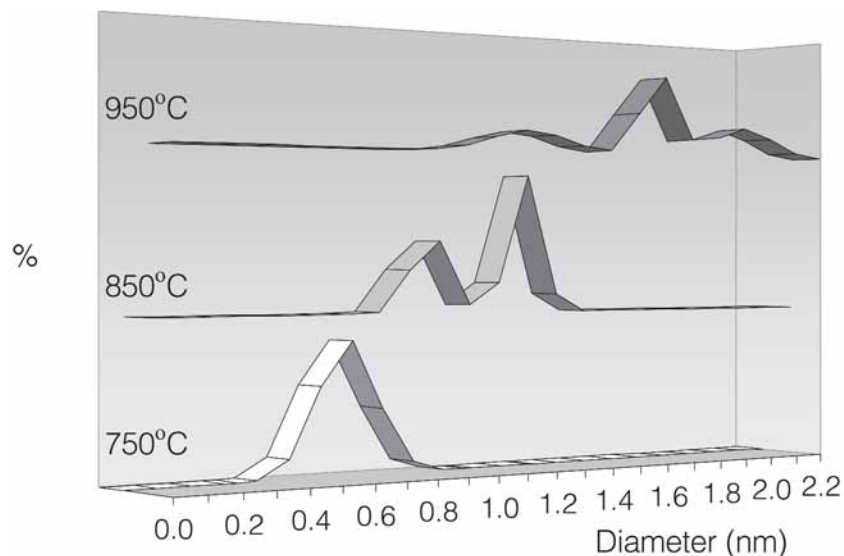


Fig. 7. Diameter distribution of SWNTs produced by CO disproportionation at three different temperatures over a selective Co–Mo (1:3)/SiO₂ catalyst, as obtained from TEM micrographs.

3.4. Incorporating H₂ in the Feed

As proposed above, the formation of embryos precedes the growth of SWNTs during the CVD process and the size of these embryos determines the diameter of the formed SWNT. The size of the embryos will be the result of the competition between metal cluster agglomeration and nanotube growth. If we add hydrogen to the CO feed, the fugacity of carbonaceous species on the surface will be reduced by the presence of hydrogen in the gas phase; in other words, active hydrogen atoms on the surface will reduce the carbon concentration of the particle by means of a process that can be envisioned as a surface “clean up.” Therefore, one would expect that this reduction in carbon concentration on the surface would favor the cluster ag-

glomeration process, setting back the nanotube growth by delaying the carbon nucleation process. As a result, depending on the hydrogen concentration we may observe an increase in nanotube diameter at low H₂ concentrations or even a loss in nanotube selectivity compared with that of nanofibers when the particle diameter becomes too large to form embryos able to grow SWNTs.

To test this hypothesis, we conducted the decomposition of CO at 750 °C. adding different H₂ to the feed ranging from 2 to 10% during the synthesis of SWNTs over a selective Co–Mo/SiO₂. To characterize the SWNTs obtained, Raman spectroscopy was performed using the three different laser excitation energies mentioned above. Figure 8 shows the Raman spectra of the product obtained when three different concentrations of hydrogen were added to the feed, using a laser excitation wavelength of 633 nm. From analysis of the intensities of the D and G bands, it becomes clear that the selectivity to SWNTs has been greatly reduced by the presence of hydrogen in the feed. The TEM observations were in perfect agreement with these conclusions. They showed a higher density of MWNTs and graphite on the samples obtained with H₂ concentrations above 6%. As anticipated above, this loss in nanotube selectivity originates from a large increase in the particle diameter in such a way that it becomes too large to form embryos able to grow SWNTs. In contrast, these large clusters generate MWNTs and graphitic fibers.

From Figure 8 a more subtle change on the RBM region can be observed when the amount of H₂ to the feed increases from 0 to 6%. The product obtained without any hydrogen present in the feed exhibits a dominant peak centered at around 278 cm⁻¹, which would correspond to a nanotube diameter of approximately 0.85.³⁰ When 6% of hydrogen is present in the feed a new peak becomes domi-

RESEARCH ARTICLE

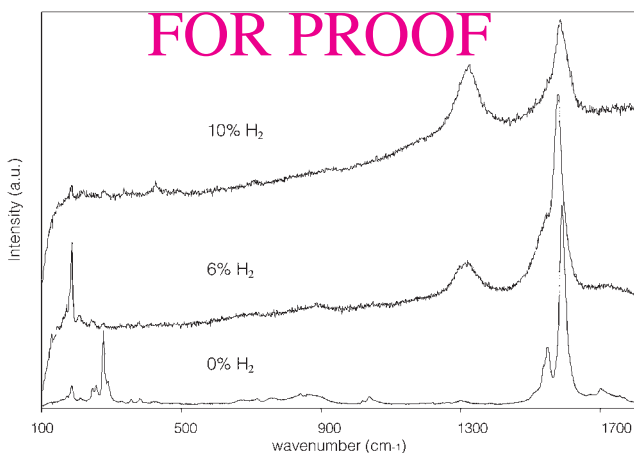


Fig. 8. Raman spectra of the SWNT growth at 750 °C over a Co–Mo (1:3)/SiO₂ catalyst by CO disproportionation adding three different amounts of H₂ to the reaction feedstock. The laser excitation line was 633 nm.

Table V. Observed positions of the radial breathing mode Raman bands for the SWNT obtained by disproportionation of CO at 750 °C over a Co–Mo (1:3)/SiO₂ catalyst with different amounts of H₂ added to the reaction feedstock.^a

Laser line	Amount of H ₂ added to the feed							
	0% H ₂		2% H ₂		4% H ₂		6% H ₂	
	RBM position (cm ⁻¹)	Diameter (nm)	RBM position (cm ⁻¹)	Diameter (nm)	RBM position (cm ⁻¹)	Diameter (nm)	RBM position (cm ⁻¹)	Diameter (nm)
633 nm	284	0.83	284	0.83	284	0.83	188	1.29
	256	0.92	188	1.29	188	1.29	215	1.12
	237	1.00	237	1.00	177	1.37	173	1.41
514 nm	264	0.89	264	0.89	258	0.92	169	1.45
	249	0.95	188	1.29	171	1.43	172	1.42
			169	1.45			202	1.19
488 nm	298	0.79	298	0.79	250	0.95	250	0.95
	249	0.95	250	0.95	238	1.00	177	1.37
	244	0.97	197	1.23	199	1.21	160	1.53

^aThe laser excitation lines were 633, 514, and 488 nm.

nant at lower wavenumbers (188 cm⁻¹), clearly indicating the appearance of nanotubes of larger diameter. Again, due to the resonant character of the Raman spectra of SWNTs, the diameter values obtained by the analysis of the breathing mode band from the Raman spectra acquired using only one laser energy may not represent the whole range of nanotube diameters other than the subset of nanotubes that are in resonance with the laser energy. Therefore, to get information that is more representative of the diameter distribution of the SWNTs in the sample, it was necessary to probe the SWNTs with several excitation energies. Table V shows the breathing mode range of frequencies in the Raman spectra obtained with three different laser excitation energies on the same SWNT samples. Although the observed peak positions for a given sample depends on the laser excitation energy, the same trend is undoubtedly observed at all energies. The bands clearly shift to lower wavenumbers as the concentration of hydrogen in the feed increased, showing an increase in SWNT diameter as the concentration of H₂ in the feed is raised.

This result is in perfect agreement with our initial hypothesis. As proposed above, at the early stages of the reaction Co atoms released from their interaction with Mo begin to coalesce, forming mobile clusters. Upon carbon bombardment from the gas phase the clusters lead to C-rich embryos that originate the growth of SWNTs. When a small amount of hydrogen is added to the feed, the rate of sintering of Co clusters may not be affected, but the carbon nucleation process may be delayed when the surface carbon fugacity is reduced. Therefore, a higher density of larger metal clusters should occur when the hydrogen concentration in the feed is increased. These larger clusters are then responsible for the formation of larger embryos, and in turn, nanotubes of larger diameter.

Acknowledgments: This research was conducted with financial support from the Department of Energy, Office of

Basic Energy Sciences (grant No. DE-FG03-02ER15345). Technical support from the personnel at NSLS, Brookhaven National Lab for the EXAFS experiments is gratefully acknowledged. One of us (J. E. H.) thanks the Fulbright-CAREC program for a scholarship.

References and Notes

1. A. Thess, R. Lee, P. Nikolaev, H. Dai, P. Petit, J. Robert, C. Xu, Y. H. Lee, S. G. Kim, A. G. Rinzler, D. T. Colbert, G. E. Scuseria, D. Tomanek, J. E. Fischer, and R. E. Smalley, *Science* 273, 483 (1996).
2. B. Kitiyanan, W. E. Alvarez, J. H. Harwell, and D. E. Resasco, *Chem. Phys. Lett.* 317, 497 (2000).
3. J. E. Herrera, L. Balzano, A. Borgna, W. E. Alvarez, and D. E. Resasco, *J. Catal.* 204, 129 (2001).
4. D. L. Trim, *Design of Industrial Catalysts*, Chemical Engineering Monographs 11, Elsevier, Amsterdam (1980), p. 107.
5. X. P. Gao, X. Qin, F. Wu, H. Liu, Y. Lan, S. S. Fan, H. T. Yuan, D. Y. Song, and P. W. Shen, *Chem. Phys. Lett.* 327, 271 (2000).
6. P. Coquay, A. Peigney, E. De Grave, R. E. Vandenberghe, and C. J. Laurent, *J. Phys. Chem. B* 106, 13199 (2002).
7. S. Delpeux, K. Szostak, E. Frackowiak, S. Bonnamy, and F. Beguin, *J. Nanosci. Nanotech.* 2, 481 (2002).
8. G. G. Tibbetts, D. W. Gorkiewicz, and R. L. Alig, *Carbon* 31, 809 (1993).
9. A. Andriotis, M. Menon, and G. Froudakis, *Phys. Rev. Lett.* 85, 3193 (2000).
10. (a) C. Laurent, E. Flahaut, A. Peigney, and A. Rousset, *New J. Chem.* 22, 1229 (1998); (b) A. Peigney, P. Coquay, E. Flahaut, R. E. Vandenberghe, E. De Grave, and C. Laurent, *J. Phys. Chem. B* 105, 9699 (2001); (c) C. Laurent, A. Peigney, E. Flahaut, and A. Rousset, *Mater. Res. Bull.* 35, 661 (2000).
11. W. E. Alvarez, B. Kitiyanan, A. Borgna, and D. E. Resasco, *Carbon* 39, 547 (2001).
12. W. E. Alvarez, F. Pompeo, J. E. Herrera, L. Balzano, and D. E. Resasco, *Chem. Mater.* 14, 1853 (2002).
13. J. E. Herrera and D. E. Resasco, *J. Phys. Chem.* 107, 3738 (2003).
14. R. Saito, M. Fujita, G. Dresselhaus and M. S. Dresselhaus, *Appl. Phys. Lett.* 60, 2204 (1992).
15. M. A. Pimenta, A. Jorio, S. D. M. Brown, A. G. Souza Filho, G. Dresselhaus, J. H. Hafner, C. M. Lieber, R. Saito, and M. S. Dresselhaus, *Phys. Rev. B* 64, 41401R (2001).

16. A. M. Rao, E. Richter, S. Bandow, B. Chase, P. C. Eklund, K. A. Williams, S. Fang, K. Subbaswamy, M. Menon, A. Thess, R. E Smalley, G. Dresselhaus, and M. S. Dresselhaus, *Science* 275, 185 (1997).
17. R. S. Weber, *J. Catal.* 151, 470 (1995).
18. H. Kasper, *Monatsh. Chem.* 98, 2104 (1967).
19. P. Gajardo, P. Grange, and B. Delmon, *J. Phys. Chem.* 83, 1771 (1979).
20. V. G. Hadjiev, M. N. Iliev, and I. V. Vergilov, *J. Phys. C: Solid State Phys.* 21, L199 (1988).
21. G. Mestl and T. K. K. Srinivasan, *Chem. Rev. Sci. Eng.* 40, 451 (1998).
22. F. R. Brown, L. E. Makovsky, and K. H. Rhee, *J. Catal.* 50, 162 (1977).
23. H. Topsøe, B. S. Clausen, R. Candia, C. Wivel, and S. Mørup, *Bull. Soc. Chim. Belg.* 12, 1187 (1981).
24. H. Topsøe, B. S. Clausen, N. Burriesci, R. Candia, and S. Mørup, in *Preparation of Catalysts II*, edited by B. Delmon, P. Grange, P. A. Jacobs, and G. Poncelet, Elsevier, Amsterdam (1979), p. 479.
25. M. de Boer, E. P. F. M. Koch, R. J. Blaauw, E. R. Stobbe, A. N. J. M. Hoffmann, L. A. Boot, A. J. van Dillen, and J. W. Geus, *Solid State Ionics* 63, 736 (1993).
26. Z. Li, Y. Fu, J. Bao, M. Jiang, T. Hu, T. Liu, and Y.-N. Xie, *Appl. Catal. A: Gen.* 220, 21 (2001).
27. G. M. Clark and W. P. Doyle, *Spectrochim. Acta* 22, 1441 (1966).
28. F. Trifiro, P. Centola, and I. Pasquon, *J. Catal.* 10, 86 (1968).
29. W. Kuang, Y. Fan, K. Chen, and Y. Chen, *J. Catal.* 186, 310 (1999).
30. S. Rols, A. Righi, L. Alvarez, E. Anglaret, R. Almairac, C. Journet, P. Bernier, J. L. Sauvajol, A. M. Benito, W. K. Maser, E. Munoz, M. T. Martinez, G. F. de la Fuente, A. Girard, and J. C. Ameline, *Eur. Phys. J. B* 18, 201 (2000).
31. A. M. Rao, J. Chen, E. Richter, U. Schlecht, P. C. Eklund, R. C. Haddon, U. D. Venkateswaran, Y.-K. Kwon, and D. Tomanek, *Phys. Rev. Lett.* 86, 3895 (2001).
32. C. L. Cheung, A. Kurtz, H. Park, and C. M. Lieber, *J. Phys. Chem. B* 106, 2429 (2003).

Received: 15 April 2003. Revised/Accepted: 22 July 2003.